NURETH-21 21st International Topical Meeting on Nuclear Reactor Thermal Hydraulics
August 31 (Sun) - September 5 (Fri), 2025
BEXCO · Busan, Korea
www.nureth-21.org

Assessment of Heat Flux Partitioning Approaches for the Prediction of Subcooled Flow Boiling

Omid Bidar and Marco Colombo
School of Mechanical, Aerospace and Civil Engineering, University of Sheffield
Western Bank, Sheffield S10 2TN, United Kingdom
o.bidar@sheffield.ac.uk; m.colombo@sheffield.ac.uk

ABSTRACT

This paper presents a point-averaged, zero-dimensional framework for nucleate boiling heat transfer, enabling systematic assessment of multiple heat flux partitioning (HFP) models in tandem with diverse bubble dynamics sub-models, often used in multiphase CFD to predict subcooled flow boiling. HFP models decompose the total heat transfer into individual components characterising various heat transfer mechanisms, such as evaporation, quenching and single-phase convection. This approach relies on sub-models for parameters like bubble departure diameter and frequency to capture these mechanisms accurately. We propose a computationally efficient way to test a large number of sub-models and explore thousands of sub-model combinations using the zero-dimensional framework. The framework also avoids having to account for the coupling with interface transfer closures or population balance models, that makes assessing boiling models inside multiphase CFD challenging. Comparisons with experimental data expose the strengths and limitations of the different model formulations, highlighting the critical impact of sub-model choice on the predictive accuracy. Through these analyses, the point-averaged approach provides valuable guidance for refining model closures and targeting further validation.

KEYWORDS
Subcooled flow boiling; heat flux partitioning; boiling models; bubble dynamic models.

1. INTRODUCTION

Nucleate boiling is an important process in nuclear thermal hydraulics and the critical heat flux (CHF) remains one of the most important safety limits in water-cooled nuclear reactors. Reliable predictions of heat transfer rates and the CHF remain challenging due to the complexity of the boiling process, the not yet fully understood interaction between the heated surface and the working fluid, and the interplay between multiple variables such as thermophysical properties, operating conditions and surface chemistry.

In the last few decades, computational fluid dynamics models based on the multifluid Eulerian-Eulerian method have been developed to simulate three-dimensional boiling flows in complex geometries. Multifluid models are developed by averaging the local and instantaneous velocity and phase distribution. The averaging process filters out interface position and lengthscale, and interface and turbulent transport and exchange processes are modelled with numerous closure relations [1, 2].

In Eulerian-Eulerian models, the heat flux partitioning (HFP) approach is commonly used to model the wall boiling process. In the HFP approach, the heat transfer is typically modelled as the sum of several contributing mechanisms, such as evaporation, quenching, and single-phase heat transfer [3]. Fundamental quantities characterising bubble dynamics, such as bubble nucleation site density, departure diameter, departure frequency, wait and growth times, are required to model the evaporation heat transfer mechanism in HFP models. A plethora of empirical,

semi-empirical, and mechanistic models have been introduced to evaluate these quantities [4]. However, their predictive capabilities are limited due to the models' inability to capture the complex interdependency between the numerous bubble dynamics quantities, overfitting of the various model parameters on limited experimental data, and epistemological uncertainties due to incomplete understanding of the underlying flow physics [5, 6, 7].

Over the years, various studies have been conducted to assess the predictive capabilities of multifluid CFD models, focusing on various aspects of the modelling framework, including assessments of the HFP closure models (e.g. [5, 7]), interfacial area transport modelling (e.g. [8, 9]), bubble coalescence and break-up models (e.g. [10, 9]) and turbulence closures (e.g. [11]). When multifluid CFD simulations are used to assess the accuracy of HFP approaches, each closure model, whether it addresses turbulence closures, interfacial forces or bubble coalescence and break-up, contributes its own set of uncertainties, which can all accumulate and obscure the specific uncertainties arising from the boiling model. Even in studies that specifically focus on the predictive capability of boiling models, discrepancies attributable to the turbulence closure or interfacial area transport equations may dominate, making it difficult to isolate the behaviour of individual bubble dynamics sub-models. Furthermore, systematically exploring every combination of heat flux partitioning method with each bubble parameter sub-model is computationally prohibitive in the context of CFD, since the range of possible sub-model configurations can yield thousands of distinct simulation scenarios.

A complementary, computationally efficient strategy is to conduct point-averaged simulations, e.g. [12], wherein boiling phenomena are modelled at a point representative of the heater surface average conditions rather than across a full three-dimensional flow domain. This allows to represent the boiling models as explicit functions of the wall superheat, flow conditions, characteristic length scale, fluid and surface thermophysical properties, while eliminating the need for iterative solution methods. Although the zero-dimensional approach neglects any detailed spatio-temporal flow analysis, it offers a practical approach for isolating and rapidly testing different boiling HFP methods and sub-models (e.g. a typical 3D multiphase Eulerian-Eulerian simulation in a pipe may take minutes to hours, whereas a point-averaged prediction runtime is of the order of milliseconds). Comparing point-averaged model predictions against experimental measurement, e.g. using boiling curves, can be really useful for the selection or refinement of HFP frameworks and sub-model combinations before undertaking more resource-intensive, multiphase CFD simulations.

Furthermore, recent experimental advances offer increasingly detailed measurements of the boiling heat transfer process. High-resolution imaging methods, coupled with IR thermography, specialised optical diagnostics and advanced post-processing techniques, enable not only measurements of heat fluxes on surfaces, but can also capture fundamental bubble dynamics parameters (e.g. nucleation site density, bubble departure diameters and frequencies, etc.) and estimate the individual heat transfer mechanisms ([13, 14, 15]), allowing detailed assessment of boiling models based on the HFP approach. Zero-dimensional, point-based models can effectively take advantage of these advanced measurements, which are often obtained in small-scale, controlled experiments not easy to model with multifluid CFD.

In this work, we develop and implement in a zero-dimensional MATLAB framework different HFP models alongside frequently used sub-models for bubble dynamics parameters. The models are assessed leveraging recent subcooled flow boiling experimental data. Limitations and directions for the future improvement of boiling frameworks implemented in Eulerian-Eulerian CFD models are highlighted and discussed. The rest of the paper is structured as follows: section 2 presents the heat flux partitioning models, section 3 provides all the sub-models for

bubble dynamics parameters, section 4 and 5 outlines the MATLAB implementation, test cases and presents results, respectively, with section 6 providing key conclusions and future work.

2. HEAT FLUX PARTITIONING

The boiling process begins with nucleation at microscopic cavities on the heated surface, where trapped gas initiates bubble formation once the wall reaches the required amount of superheat. As bubbles nucleate, they grow rapidly, trapping a thin microlayer of liquid against the wall, which evaporates adding to heat transfer. After this initial growth, a dry spot forms under the bubble, and the wall temperature rises locally until the bubble departs. Once the bubble detaches, fresh liquid rewets this area, rapidly cooling it through transient conduction. Depending on conditions, bubbles may either detach directly or slide along the surface before lifting off, with sliding bubbles enhancing heat transfer by disrupting the boundary layer. At high heat fluxes, bubbles interact more frequently, merging or detaching early due to crowding, which alters the heat transfer dynamics. In bubble-free areas, single-phase convection continues, with additional turbulence from surface roughness contributing to heat transfer [16]. HFP models represent these heat transfer mechanisms as individual contributors to the total heat flux.

One of the most commonly used HFP models is the Rensselaer Polytechnic Institute (RPI) model [17], which represents the heat transfer as the sum of evaporation, quenching, and single-phase convection, see HFP-1 model in Table 1. More recent HFP models have attempted to capture further details, such as the effects of sliding bubbles, which is not accounted for in the RPI model. One of such models that will be considered in this work is the model developed at MIT [16, 12] (HFP-2 in Table 1).

Table 1. Heat flux partitioning models used in this work. For symbol descriptions refer to the nomenclature section.

HFP-1: *RPI* [17]

$$q'' = q''_c + q''_q + q''_e,$$
$$q''_c = h_c\left(1 - \frac{\pi}{4} D_d^2\, K\, \overline{N_b}\right)(\Delta T_w + \Delta T_{\text{sub}}),$$
$$q''_q = t_w\, f\, \frac{\pi}{4} D_d^2\, K\, \overline{N_b}\, \frac{2\, k_l\, (\Delta T_w + \Delta T_{\text{sub}})}{\sqrt{\pi\, t_w\, k_l/(\rho_l\, c_{p,l})}},$$
$$q''_e = \frac{\pi}{6}\, \rho_v\, h_{lv}\, D_d^3\, f\, \overline{N_b},$$
$$K = 4.8\, \exp\!\left(-\text{Ja}/80\right) \quad [18].$$

HFP-2: *MIT* [12]

$$q'' = q''_c + q''_{sc} + q''_e, \quad q''_e = q''_{ml} + q''_{in},$$
$$q''_c = \left(1 - S_{sl}\right) h_c\, \left(\Delta T_w + \Delta T_{\text{sub}}\right),$$
$$q''_{sc} = \frac{k_l}{\sqrt{\pi\, \eta_l\, t^*}}\, S_{sl}\, \left(\Delta T_w + \Delta T_{\text{sub}}\right),$$
$$q''_{ml} = \rho_l\, h_{lv}\, f\, \overline{N_b} \left\{ \delta_{ml}\, D_{ml}^2\, \frac{\pi}{12} \left[2 - \left(\left(\frac{D_{dry}}{D_{ml}} \right)^2 + \frac{D_{dry}}{D_{ml}} \right) \right] \right\},$$
$$q''_{in} = \frac{4}{3}\, \pi \left(\frac{D_{in}}{2} \right)^3 \rho_v\, h_{lv}\, f\, \overline{N_b},$$
$$\frac{D_{dry}}{D_{ml}} = \max(0.1237\text{Ca}^{-0.373} \sin\theta, 1), \quad D_{in} = \frac{D_{dry}}{D_{ml}} D_d,$$

Continued on next page

Table 1. (*Continued*)

$$D_{ml} = \frac{D_{in}}{2}, \quad \delta_{ml} = 4 \times 10^{-6}\sqrt{\frac{\mathrm{Ca}}{\mathrm{Ca}_0}}, \quad S_{sl} = \min(1, A_{sl}\overline{N_b}t^* f),$$
$$A_{sl} = \frac{1}{\sqrt{\overline{N_b}}}\left(\frac{D_{lo}+D_d}{2}\right), \quad t^* = \left(\frac{k_l}{h_c}\right)^2 \frac{1}{\pi\eta_l}, \quad D_{lo} = 1.2D_d.$$

3. BUBBLE PARAMETER MODELS

HFP models rely on a large number of closures to model the evaporation process such as bubble departure diameters, departure frequency, nucleation site density, growth and wait times. Many models for these parameters are available in literature, almost always developed on an empirical or semi-empirical basis. These are reviewed in detail in Ref. [4]. In this work, we have implemented a number of them that are outlined in Table 2.

Table 2. List of the bubble parameter models used in the present work.

Author(s)	**Model/Correlation**
	Bubble Departure Diameters (BDD)
Fritz [19]	$D_d = 0.0208\theta\sqrt{\frac{\sigma}{g(\rho_l-\rho_v)}}$
Ruckenstein [20]	$D_d = \left[\frac{3\pi^2\rho_l\alpha_l^2 g^{0.5}(\rho_l-\rho_v)^{0.5}}{\sigma^{3/2}}\right]\mathrm{Ja}^{4/3}\left[\frac{2\sigma}{g(\rho_l-\rho_v)}\right]^{1/2}$
Van Stralen & Zijl [21]	$D_d = 2.63\left(\frac{\mathrm{Ja}\alpha_l^2}{g}\right)^{1/3}\left[1+\left(\frac{2\pi}{3\mathrm{Ja}}\right)^{0.5}\right]^{1/4}$
MIT [12]	$D_d = 18.9\times10^{-6}\left(\frac{\rho_l-\rho_v}{\rho_v}\right)^{0.27}\mathrm{Ja}_{\mathrm{sup}}^{0.75}(1+\mathrm{Ja}_{\mathrm{sub}})^{-0.3}u^{-0.26}$
Kocamustafaogullari [22]	$D_d = 2.64\times10^{-5}\left[\frac{\sigma}{g(\rho_l-\rho_v)}\right]^{\frac{1}{2}}\left(\frac{\rho_l-\rho_v}{\rho_l}\right)^{0.9}$
Tolubinsky & Kostanchuk [23]	$D_d = \min\left(0.0014, 0.0006\exp\left(-\frac{\Delta T_{\mathrm{sub}}}{45}\right)\right)$
	Bubble Departure Frequency (BDF)
Cole [24]	$fD_d^{0.5} = \left[\frac{4g(\rho_l-\rho_v)}{3\rho_l}\right]^{1/2}$
Stephan [25]	$fD_d = \frac{1}{\pi}\left[\frac{g}{2}\left(D_d+\frac{4\sigma}{\rho_l g D_d}\right)\right]^{1/2}$
Zuber [26]	$fD_d = \left(\frac{1.18}{2}\right)\left[\frac{\sigma g(\rho_l-\rho_v)}{\rho_l^2}\right]^{1/4}$
MIT [12]	$f = \frac{1}{t_w+t_g}$
	Nucleation Site Density (NSD)
Hibiki & Ishii [27]	$\overline{N_b} = N_0\left(1-\exp\left(-\frac{\theta^2}{8\mu^2}\right)\right)\left[\exp\left(\frac{f(\rho^+)\lambda'}{R_c}\right)-1\right],$
	$R_c = \frac{2\sigma[1+(\rho_v/\rho_l)]/P}{\exp[h_{lv}(T_g-T_{\mathrm{sat}})/(R_g T_g T_{\mathrm{sat}})]-1},$
	$\rho^+ = \log\left(\frac{\rho_l-\rho_v}{\rho_v}\right),$
	$f(\rho^+) = -0.01064+0.48246\rho^+-0.22712(\rho^+)^2+0.05468(\rho^+)^3,$

Continued on next page

Table 2. (*Continued*)

Author(s)	**Correlation**
	$N_0 = 4.72 \times 10^5$ sites/m^2, $\mu = 0.722$ rad, $\lambda' = 2.56 \times 10^{-6}$ m.
Hibiki & Ishii MIT [7]	$\overline{N_b} = \overline{N_b}_{\mathrm{HI}} \exp\left[-N_0 \pi \left(\frac{D_d}{2}\right)^2\right]$,
	$\overline{N_b} = \begin{cases} \overline{N_b}_{\mathrm{HI}}, & A < e^{-1}, \\ \frac{0.2689 N_0 \overline{N_b}_{\mathrm{HI}} + 0.2690}{N_0}, & e^{-1} \le A \le e, \\ \frac{\ln(N_0 \overline{N_b}_{\mathrm{HI}}) - \ln(\ln(N_0 \overline{N_b}_{\mathrm{HI}}))}{N_0}, & A > e \end{cases}$
	$A = N_0 \overline{N_b}_{\mathrm{HI}}, \quad N_0 = f t_g \overline{N_b}_{\mathrm{HI}}.$
	$\overline{N_b}_{\mathrm{HI}}$ is the NSD from the Hibiki-Ishii model.
Lemmert & Chawla [28]	$\overline{N_b} = (185 \Delta T_w)^{1.805}$
	Bubble Growth Time (BGT)
MIT [12]	$t_g = \left(\frac{D_d}{4K}\right)^2$,
	$K = \mathrm{Ja}_{\mathrm{sup}} \sqrt{\eta_f} \left(\frac{1.243}{\sqrt{\mathrm{Pr}_f}} - \min\left(0.5 \frac{1.243}{\sqrt{\mathrm{Pr}_f}}, 0.0977 \frac{\Delta T_{\mathrm{sub}}}{\Delta T_{\mathrm{w}}}\right)\right)$[7].
Lee et al. [29]	$t_g = 67.5 \mathrm{Ja} \alpha \rho_l \frac{D_d}{\sigma}$
	Bubble Wait Time (BWT)
MIT [12]	$t_w = \frac{0.0061 \mathrm{Ja}_{\mathrm{sub}}^{0.63}}{\Delta T_w}$
Van Stralen et al. [30]	$t_w = 3 t_g$
Churchill & Chu [31]	$\mathrm{Nu} = \left\{ \frac{0.825 + 0.387 \mathrm{Ra}^{1/6}}{\left[1 + (0.492/\mathrm{Pr})^{9/16}\right]^{8/27}} \right\}^2$
Gnielinski [32]	$\mathrm{Nu} = \frac{(f_{\mathrm{Darcy}}/8)(\mathrm{Re}_D - 1000)\mathrm{Pr}}{1 + 12.7\sqrt{f_{\mathrm{Darcy}}/8}(\mathrm{Pr}^{2/3} - 1)}$

4. MATLAB IMPLEMENTATION AND TEST CASES

The models outlined are implemented in MATLAB in a module we call XBOIL. The code is structured with modular functions which take the wall superheat and other operating parameters as inputs, and output bubble parameters and heat fluxes. The modular implementation allows the easy selection between available models and the additions of other sub-models, and supports sweepings across all different model combinations, along with graphical and tabular post-processing, which will be presented in the following section. We use CoolProp [33] to evaluate the thermophysical properties of fluids.

In this work, two different sets of boiling curves, where the wall superheat is measured as a function of the imposed wall heat flux, are used to evaluate the accuracy of the models. The first set of test cases are based on the experimental data by Richenderfer et al. [13]. The flow is through a rectangular channel (3×1 cm^2), with deionised water, at atmospheric pressure, 10° C of subcooling, and three mass fluxes (500, 750, and 1000 kgm^{-2}s^{-1}). The IR heater surface

is coated with indium-tin-oxide (ITO) which is used to define the thermophysical properties of the heater. The contact angle is 85° based on the data from [13]. The second dataset is based on the experimental data by Kennel et al. [34, 35]. The flow is through an annulus with a stainless steel heater. Unlike the first dataset, this dataset also considers variations in pressure, as well as the subcooling and mass fluxes.

5. RESULTS AND DISCUSSION

Available boiling modelling closures have been combined in a countless number of configurations in previous works. The fast-running XBOIL MATLAB framework allowed us to take an agnostic approach and test all the 1,152 possible configurations of the models in Section 2. Fig. 1 presents the range of predictions (based on the minimum-maximum bounds) for up to the top 400 models, ranked based on their mean-squared error (MSE) for one of the experimental cases of Richenderfer et al. [13]. The variability in results illustrates the inherent sensitivity of the HFP model predictions to the choice of the boiling sub-models.

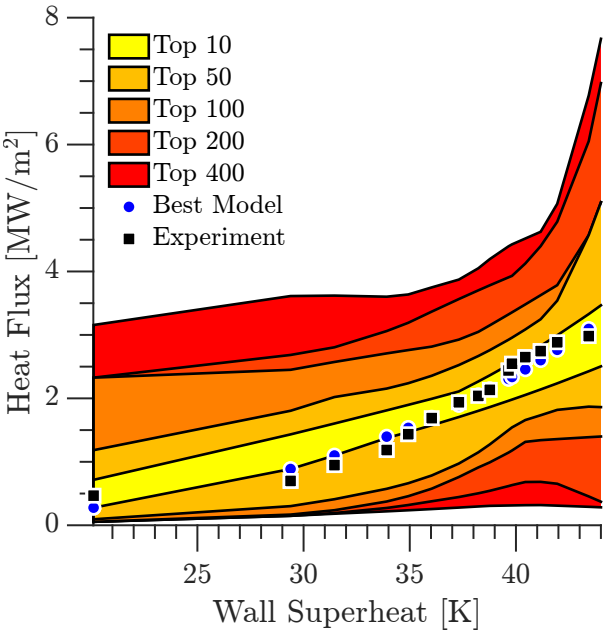

Figure 1. Min-max heat flux predictions for Richenderfer et al. [13] case at: $p = 1.0$ bar, $u = 0.8$ ms^{-1}, $T_{\text{sub}} = 10.0$ K.

Table 3. Best model combinations for each test case.

	Cases					
Params	$p = 1.0$ bar $u = 0.5$ ms^{-1} $T_{\text{sub}} = 10.0$ K	$p = 1.0$ bar $u = 0.8$ ms^{-1} $T_{\text{sub}} = 10.0$ K	$p = 1.0$ bar $u = 1.0$ ms^{-1} $T_{\text{sub}} = 10.0$ K	$p = 2.0$ bar $u = 0.3$ ms^{-1} $T_{\text{sub}} = 27.8$ K	$p = 4.0$ bar $u = 1.2$ ms^{-1} $T_{\text{sub}} = 11.1$ K	$p = 6.0$ bar $u = 1.2$ ms^{-1} $T_{\text{sub}} = 27.8$ K
HFP	MIT	MIT	RPI	MIT	MIT	RPI
BDD	MIT	MIT	MIT	MIT	Van Stralen & Zijl	Van Stralen & Zijl
BDF	Stephan	Zuber	Cole	MIT	Stephan	Zuber
NSD	Lemmert & Chawla	Lemmert & Chawla	Hibiki & Ishii	Hibiki & Ishii MIT	Lemmert & Chawla	Hibiki & Ishii MIT
BGT	MIT	MIT	Lee et al.	MIT	Lee et al.	MIT
BWT	MIT	Van Stralen et al.	MIT	MIT	Van Stralen et al.	Van Stralen et al.
CHT	Gnielinski	Churchill & Chu	Gnielinski	Gnielinski	Gnielinski	Gnielinski

Abbreviations: HFP = heat flux partitioning; BDD = bubble departure diameter; BDF = bubble departure frequency; NSD = nucleation site density; BGT = bubble growth time; BWT = bubble wait time; CHT = (single phase) convection heat transfer.

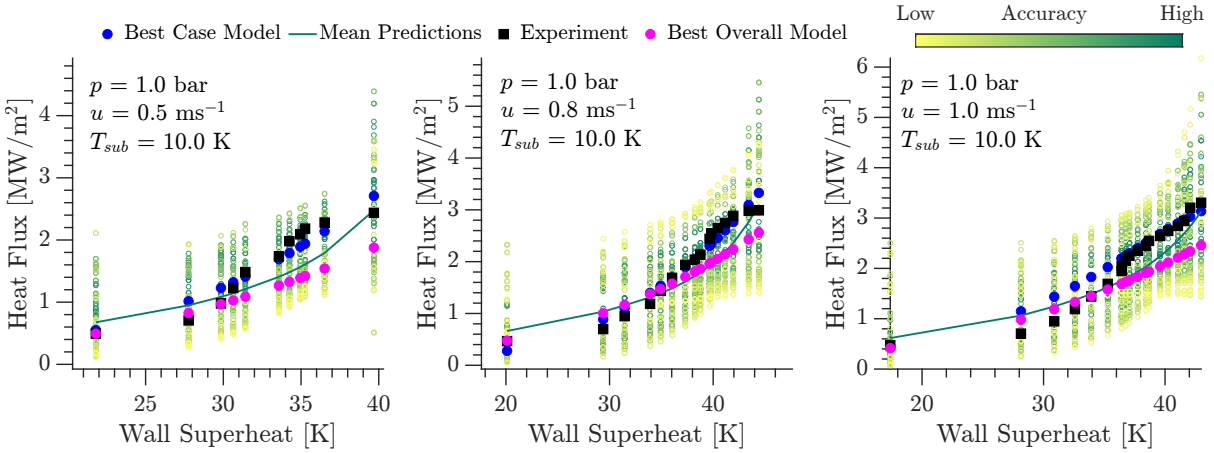

(a) Richenderfer et al. dataset [13]

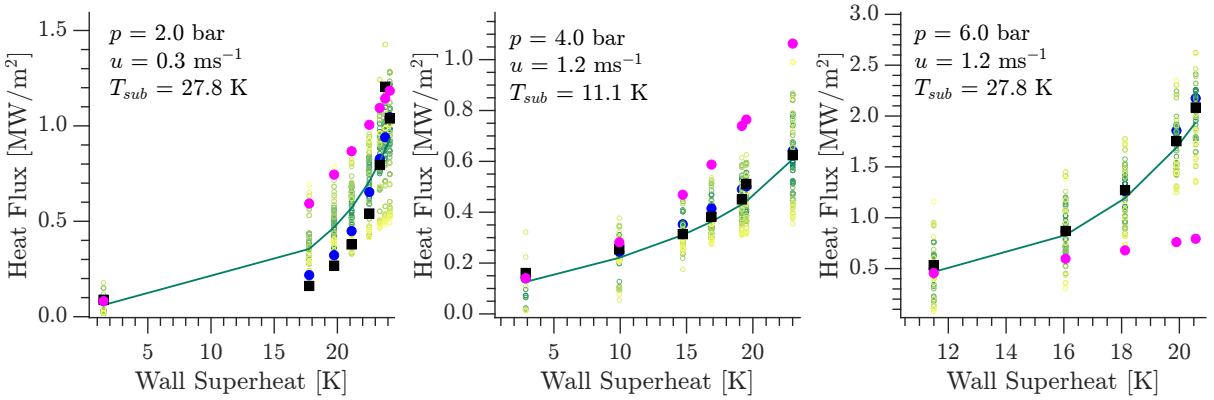

(b) Kennel dataset [34, 35]

Figure 2. Boiling curves comparing the model predictions to experimental data. Predictions with smaller MSE values are in darker shades of green, as shown in the colour bar.

The boiling curves for the six test cases are shown in Fig. 2. The curves labelled 'Best Case Model' refers to the model configurations with the smallest mean-squared error (MSE) relative to the experimental measurements of that particular case. These best model configurations for each case are shown in Table 3. The best overall sub-model is determined by analysing the frequency of sub-models across all the test cases. For each case, the top N models (e.g., 100) with the lowest MSE are identified. From these top models, the frequency of each sub-model (e.g., for heat flux partitioning, bubble departure diameter, nucleation site density, etc.) is counted. The sub-model that appears most frequently in the best-performing models for each category is chosen as the best overall sub-model, with the results presented in Table 4. The boiling curves illustrate that it is possible to replicate the experimental heat fluxes with a satisfactory level of accuracy when using specific model configurations (i.e. the 'best case models' shown in Table 3). However, it is difficult to achieve it with the same model configuration (i.e. the 'best overall model' shown in Table 4).

The MIT heat flux partitioning model out-performs the RPI model, which may highlight the importance of including bubble sliding effects for a better representation of the heat transfer mechanisms. For the Richenderfer et al. dataset [13], with constant pressure and subcooling, the MIT departure diameter models outperform the others. On the other hand, for the Kennel dataset [34], with higher pressures and varying subcooling, the Van Stralen & Zijl departure diameter model provides the best heat flux predictions. First, this highlights the sensitivity of the models to flow conditions, and second, it is interesting to note that both models include a

Jakob number dependency which has been shown to correlate to the departure diameter [36, 37]. In terms of the bubble departure frequency, the 'best' model is difficult to discern, as all the four models implemented appear in the 'Best Case Model' in Table 3.

Table 4. Frequency of sub-models in the top 100 configurations used for selecting the best overall configuration across all test cases. The percentages indicate how often each sub-model appears in the top-ranked models. Models are ordered from highest to lowest frequency, therefore the first sub-model for each model category forms the 'Best Overall Model' (further highlighted in italics).

Model Type	Models	Frequency
Heat Flux Partitioning	*MIT*	54.7%
	RPI	45.3%
Bubble Departure Diameter	*Van Stralen & Zijl*	30.2%
	MIT	28.3%
	Tolubinsky & Kostanchuk	26.2%
	Fritz	8.3%
	Ruckenstein	6.3%
	Kocamustafaogullari	0.07%
Bubble Departure Frequency	*Stephan*	35.3%
	Zuber	23.7%
	Cole	22.5%
	MIT	18.5%
Nucleation Site Density	*Lemmert & Chawla*	41.7%
	Hibiki & Ishii MIT	31.8%
	Hibiki & Ishii	26.5%
Bubble Growth Time	*Lee et al.*	56.0%
	MIT	44.0%
Bubble Wait Time	*MIT*	51.3%
	Van Stralen et al.	48.7%
CHT: Nusselt Number Correlation	*Gnielinski*	57.3%
	Churchill & Chu	42.7%

In terms of the growth time models, the MIT correlation is frequently selected in Table 3. This may be explained by the fact that the MIT model has been developed to account for bubble growth due to the microlayer evaporation, and condensation at the bubble cap as a result of the flow subcooling [12], i.e., designed to account for the bubble growth mechanisms relevant to flow boiling. Conversely, the alternative model by Lee et al. [29] was developed based on experimental data for pool boiling. For the bubble wait times, both the MIT [12] and Van Stralen et al. [30] models appear in Table 3. For the single phase convective heat transfer, the Gnielinski correlation is chosen for all cases, apart from the case with the lowest velocity, see Table 3.

For the nucleation site density, the Lemmert & Chawla correlation is frequently part of the best model configurations in Table 3. While nucleation site density measurements are not available for the Kennel dataset [34], they were measured by Richenderfer et al. [13] together with all the most important bubble parameters. These measurements allow assessing the accuracy of each closure that is summarized in Fig. 3. Despite appearing in the 'best overall model',

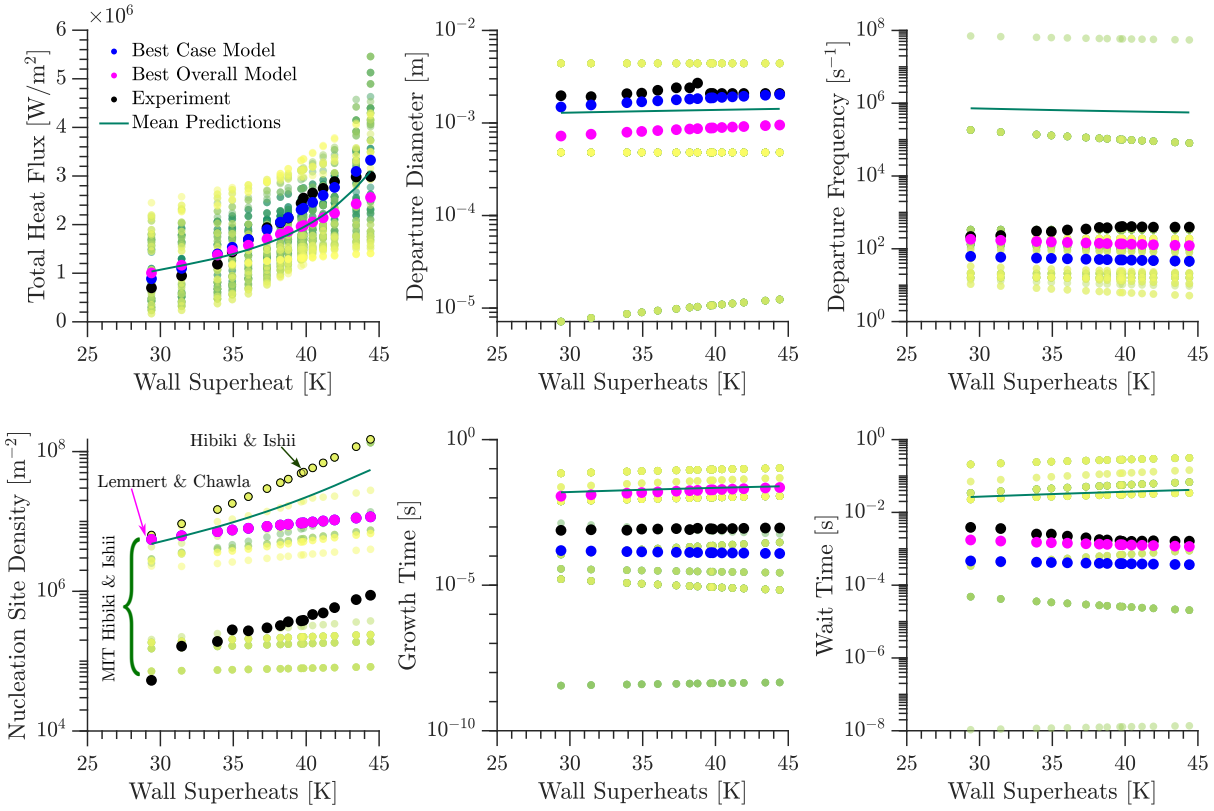

Figure 3. Comparison of the predicted and experimental total heat flux and individual bubble dynamic parameters for Richenderfer et al. [13] at $p = 1.0$ bar, $u = 0.8$ m s^{-1}, $T_{\text{sub}} = 10.0$ K.

the Lemmert & Chawla correlation significantly over-predicts the nucleation site densities, as shown for one of the cases in Fig. 3. Some of the MIT-modified Hibiki-Ishii model predictions, which account for pressure dependency and other bubble parameters such as departure diameter and frequency, which are neglected by the Lemmert & Chawla correlation, are closer to the experimental nucleation site densities (Fig. 3), however this does not necessarily lead to better heat flux predictions. This highlights the inherent challenges of the HFP approach, where heat flux predictions depend on the collective contributions of all closure models. Even when the NSD model is inaccurate, the overall heat flux predictions can remain satisfactory due to compensatory effects from other sub-models. This however leads to the lack of robustness shown by the large range of results in Fig. 1 and highlights the need to develop HFP models providing not only accurate heat flux predictions, but also built on reliable sub-models for each parameter.

Fig. 4 compares the experimental heat fluxes against the best model configurations for each case (as outlined in Table 3), and the 'best overall' configuration. For the former, 90.9% of all the data points fall within the ±30% of the experimental measurements, while for the latter it drops to 78.8% within the ±30%. Since the ±30% threshold as a measure of model accuracy is somewhat arbitrary, Table 5 reports values considering some other threshold percentages. The 'best overall' configuration is particularly inaccurate at $p = 6.0$ bar and the highest value of subcooling $T_{sub} = 27.8$ K, where it under-predicts the heat fluxes (Fig. 2). This highlights the need to include data over a wider range of parameters in future, as the current 'best overall' configuration seems biased towards the conditions of Richenderfer et al. [13]. In addition, the frequency analysis approach to identify the 'best overall' configuration, while easy to implement, assumes the sub-models are independent, which is not the case as demonstrated thus far. An alternative approach that will be investigated in the future can be as follows: once the top 100 sub-model configurations for each case is identifield, pool these into a list of potential 'best

overall' configurations. Each configuration in the list is then tested across all the cases, and the one with the smallest aggregate error (e.g. the sum of MSE across all the cases) is chosen as the 'best overall' configuration.

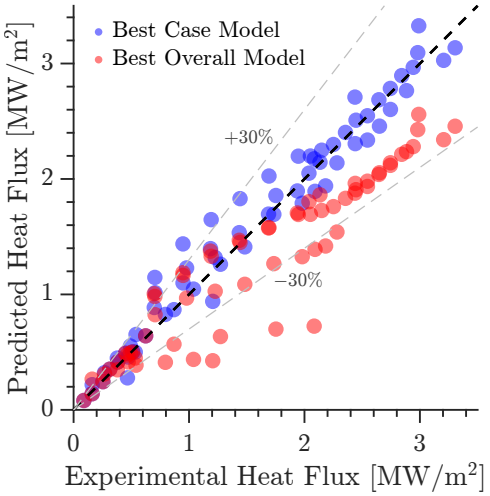

Figure 4. Scatter plot for all the test cases comparing the predicted and experimental total heat fluxes. Best Case Model refers to results obtained for each case with the related best model in Table 3, while the Best Overall Model is shown in Table 4.

Table 5. Fraction of points within a certain percentage ϵ of the experimental values for the test cases.

	$\pm\epsilon\%$					
Scenario	$\epsilon = 5$	$\epsilon = 10$	$\epsilon = 20$	$\epsilon = 30$	$\epsilon = 50$	$\epsilon = 75$
Best case model	0.39	0.65	0.82	0.91	0.97	1.0
Best overall model	0.12	0.21	0.48	0.79	0.91	1.0

6. CONCLUSIONS AND FUTURE WORK

This paper presented a systematic assessment of heat flux partitioning (HFP) models and bubble dynamics sub-models within a zero-dimensional point-averaged modelling framework implemented in MATLAB. We evaluated two heat flux partitioning frameworks alongside multiple closures characterising bubble parameters such as departure diameter, departure frequency, nucleation site density, etc. By evaluating 1,152 model configurations against experimental data, we demonstrated the significant variability in predicted heat fluxes, highlighting the sensitivity of results to sub-model selection. The MIT HFP model consistently outperformed the RPI model. Similarly, the best-performing sub-models for bubble departure diameter, nucleation site density, and other parameters varied across datasets, reflecting the dependence of sub-model accuracy on flow conditions. While the best-case model selections achieved high predictive accuracy, the best overall sub-model configuration exhibited limitations, in particular at high pressure and subcooling, even in the not huge range of parameters tested. These findings demonstrate that we are still far away from developing a universal set of models (HFP and bubble dynamics sub-models) to accurately predict subcooled flow boiling. Additionally, the need for boiling models to be built on accurate individual sub-models is highlighted, in order to ensure that all the other bubble parameters are predicted accurately, alongside the total heat

flux. This is crucial for robustness and reliability.

In future work, we will expand the dataset to include pool boiling, higher pressures, greater subcooling, different working fluids, and various geometries, including both vertical and horizontal boiling, to improve modelling assessments. In addition we will perform a sensitivity analysis for flow and other parameters, such as contact angle. We will also incorporate additional heat flux partitioning and bubble dynamics sub-models, and extend the framework to model critical heat flux, enabling a unified assessment of different boiling regimes. To support broader adoption and collaboration, we plan to release the XBOIL framework as open-source software, allowing researchers to contribute new models and validate against diverse datasets. Additionally, we will explore data-driven approaches, such as machine learning, to improve closure relations and/or potentially optimise model selection. Finally, we aim to integrate these improvements and any new insights into Eulerian-Eulerian CFD simulations.

NOMENCLATURE

A_{sl}	Bubble sliding area [-]
α	Thermal diffusivity [m^2 s^{-1}]
Ca	Capillary number [-]
Ca_0	Capillary number at 1 bar, $2.16 \times 10^{-4}(\Delta T_w)^{1.216}$ [-]
c_p	Specific heat capacity at constant pressure [J kg^{-1} K^{-1}]
D_d	Bubble departure diameter [m]
D_{dry}	Dry spot diameter [m]
D_{in}	Inception diameter [m]
D_{lo}	Lift-off diameter [m]
D_{ml}	Microlayer extension diameter [m]
f	Bubble departure frequency [s^{-1}]
f_{Darcy}	Darcy friction factor [-]
g	Gravitational acceleration [m s^{-2}]
h_c	Convective heat transfer coefficient [W m^{-2} K^{-1}]
h_{lv}	Latent heat of vaporisation [J kg^{-1}]
Ja	Jakob number [-]
K	Bubble growth constant [m $s^{-1/2}$]
k_l	Thermal conductivity of liquid [W m^{-1} K^{-1}]
ν_l	Kinematic viscosity of liquid [m^2 s^{-1}]
$\overline{N_b}$	Nucleation site density [m^{-2}]
Nu	Nusselt number [-]
P	Pressure [Pa]
Pr	Prandtl number [-]
q''	Total heat flux [W m^{-2}]
q''_c	Convective heat flux [W m^{-2}]
q''_q	Quenching heat flux [W m^{-2}]
q''_e	Evaporative heat flux [W m^{-2}]
q''_{sc}	Sliding conduction heat flux [W m^{-2}]
q''_{ml}	Microlayer heat flux [W m^{-2}]
q''_{in}	Inception heat flux [W m^{-2}]
R_g	Gas constant [J mol^{-1} K^{-1}]
Ra	Rayleigh number [-]
Re	Reynolds number
η	Thermal diffusivity [J m^{-3} K^{-1}]
ρ_l	Liquid density [kg m^{-3}]

ρ_v	Vapour density [kg m^{-3}]
σ	Surface tension [N m^{-1}]
S_{sl}	Fraction of heat surface area influenced by sliding bubbles [-]
t^*	Time needed to reform the thermal boundary layer [s]
t_g	Growth time [s]
t_w	Wait time [s]
T_l	Liquid temperature [K]
T_g	Gas temperature [K]
T_w	Wall temperature [K]
ΔT_{w}	Wall superheat [K]
ΔT_{sub}	Wall subcooling [K]
T_{sat}	Saturation temperature [K]
θ	Contact angle [rad]
δ_{ml}	Microlayer thickness [m]

ACKNOWLEDGMENTS

This work was supported by the Engineering and Physical Sciences Research Council (EPSRC) award EP/X039927/1.

REFERENCES

[1] G. H. Yeoh and J. Tu, *Computational techniques for multiphase flows*, Butterworth-Heinemann (2019).

[2] R. T. Lahey Jr, E. Baglietto, and I. A. Bolotnov, "Progress in multiphase computational fluid dynamics," *Nuclear Engineering and Design*, **374**, pp. 111018 (2021).

[3] G. R. Warrier and V. K. Dhir, "Heat Transfer and Wall Heat Flux Partitioning During Subcooled Flow Nucleate Boiling—A Review," *Journal of Heat Transfer*, **128** (12), pp. 1243–1256 (2006).

[4] R. L. Mohanty and M. K. Das, "A critical review on bubble dynamics parameters influencing boiling heat transfer," *Renewable and Sustainable Energy Reviews*, **78**, pp. 466–494 (2017).

[5] M. Colombo and M. Fairweather, "Accuracy of Eulerian–Eulerian, two-fluid CFD boiling models of subcooled boiling flows," *International Journal of Heat and Mass Transfer*, **103**, pp. 28–44 (2016).

[6] G. Giustini, "Modelling of Boiling Flows for Nuclear Thermal Hydraulics Applications—A Brief Review," *Inventions*, **5** (3), pp. 47 (2020).

[7] M. Pham, G. Bois, F. Francois, and E. Baglietto, "Assessment of State-of-The-Art Multiphase Cfd Modeling for Subcooled Flow Boiling in Reactor Applications," *Nuclear Engineering and Design*, **411**, pp. 112379 (2023).

[8] C. S. Brooks and T. Hibiki, "Modeling and validation of interfacial area transport equation in subcooled boiling flow," *Journal of Nuclear Science and Technology*, **53** (8), pp. 1192–1204 (2016).

[9] M. Colombo, R. Rzehak, M. Fairweather, Y. Liao, and D. Lucas, "Benchmarking of computational fluid dynamic models for bubbly flows," *Nuclear Engineering and Design*, **375**, pp. 111075 (2021).

[10] M. Colombo and M. Fairweather, "RANS simulation of bubble coalescence and break-up in bubbly two-phase flows," *Chemical Engineering Science*, **146**, pp. 207–225 (2016).

[11] M. Colombo and M. Fairweather, "Influence of multiphase turbulence modelling on interfacial momentum transfer in two-fluid Eulerian-Eulerian CFD models of bubbly flows," *Chemical Engineering Science*, **195**, pp. 968–984 (2019).

[12] R. Kommajosyula, *Development and assessment of a physics-based model for subcooled flow boiling with application to CFD*, Ph.d. thesis, Massachusetts Institute of Technology, 2020.

[13] A. Richenderfer et al., "Investigation of subcooled flow boiling and CHF using high-resolution diagnostics," *Experimental Thermal and Fluid Science*, **99**, pp. 35–58 (2018).

[14] M. J. Inanlu et al., "Unveiling the fundamentals of flow boiling heat transfer enhancement on structured surfaces," *Science Advances*, **10** (45), pp. eadp8632 (2024).

[15] V. Voulgaropoulos, G. M. Aguiar, C. Markides, and M. Bucci, "Simultaneous laser-induced fluorescence, particle image velocimetry and infrared thermography for the investigation of the flow and heat transfer characteristics of nucleating vapour bubbles," *International Journal of Heat and Mass Transfer*, **187**, pp. 122525 (2022).

[16] L. Gilman and E. Baglietto, "A self-consistent, physics-based boiling heat transfer modeling framework for use in computational fluid dynamics," *International Journal of Multiphase Flow*, **95**, pp. 35–53 (2017).

[17] N. Kurul and M. Z. Podowski, "Multidimensional effects in forced convection subcooled boiling," *Proc. Proceeding of International Heat Transfer Conference 9*, (1990), Begellhouse.

[18] J. Tu and G. Yeoh, "On numerical modelling of low-pressure subcooled boiling flows," *International Journal of Heat and Mass Transfer*, **45** (6), pp. 1197–1209 (2002).

[19] W. Friz, "Maximum volume of vapor bubbles," *Physikalische Zeitschrift*, **36**, pp. 379–354 (1935).

[20] R. Ruckenstein, "Recent trends in boiling heat transfer research," *Applied Mechanics Reviews*, **17**, pp. 663–672 (1964).

[21] S. J. D. van Stralen and W. Zijl, "Fundamental developments in bubble dynamics," *Proc. Proceedings of the 6th International Heat Transfer Conference*, (1978).

[22] G. Kocamustafaogullari, "Pressure dependence of bubble departure diameter for water," *International Communications in Heat and Mass Transfer*, **10** (6), pp. 501–509 (1983).

[23] V. I. Tolubinsky and D. Kostanchuk, "Vapour bubbles growth rate and heat transfer intensity at subcooled water boiling," *Proc. Proceeding of International Heat Transfer Conference 4*, (1970), Begellhouse.

[24] R. Cole, "Bubble frequencies and departure volumes at subatmospheric pressures," *AIChE Journal*, **13** (4), pp. 779–783 (1967).

[25] K. Stephan, "Enhancement of Heat Transfer During Boiling," in *Heat Transfer in Condensation and Boiling*, pp. 292–301, Springer, (1992).

[26] N. Zuber, "Nucleate boiling. The region of isolated bubbles and the similarity with natural convection," *International Journal of Heat and Mass Transfer*, **6** (1), pp. 53–78 (1963).

[27] T. Hibiki and M. Ishii, "Active nucleation site density in boiling systems," *International Journal of Heat and Mass Transfer*, **46** (14), pp. 2587–2601 (2003).

[28] M. Lemmert and L. M. Chawla, "Influence of flow velocity on surface boiling heat transfer coefficient," *International Heat Transfer Conference Proceedings* (1974), Published in 1977.

[29] H. C. Lee, B. D. Oh, S. W. Bae, and M. H. Kim, "Single bubble growth in saturated pool boiling on a constant wall temperature surface," *International Journal of Multiphase Flow*, **29** (12), pp. 1857–1874 (2003).

[30] S. van Stralen, M. Sohal, R. Cole, and W. Sluyter, "Bubble growth rates in pure and binary systems: Combined effect of relaxation and evaporation microlayers," *International Journal of Heat and Mass Transfer*, **18** (3), pp. 453–467 (1975).

[31] S. W. Churchill and H. H. S. Chu, "Correlating equations for laminar and turbulent free convection from a vertical plate," *International Journal of Heat and Mass Transfer*, **18** (11), pp. 1323–1329 (1975).

[32] V. Gnielinski, "New equations for heat and mass transfer in turbulent pipe and channel flow," *International Chemical Engineering*, **16** (2), pp. 359–368 (1976).

[33] I. H. Bell, J. Wronski, S. Quoilin, and V. Lemort, "Pure and Pseudo-pure Fluid Thermophysical Property Evaluation and the Open-Source Thermophysical Property Library CoolProp," *Industrial & Engineering Chemistry Research*, **53** (6), pp. 2498–2508 (2014).

[34] W. E. Kennel, *Local boiling of water and superheating of high pressure steam in annuli*, PhD thesis, Massachusetts Institute of Technology, 1949.

[35] W. H. McAdams et al., "Heat transfer at high rates to water with surface boiling," *Industrial & Engineering Chemistry*, **41** (9), pp. 1945–1953 (1949).

[36] J. Du, C. Zhao, and H. Bo, "Investigation of bubble departure diameter in horizontal and vertical subcooled flow boiling," *International Journal of Heat and Mass Transfer*, **127**, pp. 796–805 (2018).

[37] P. Zhou, R. Huang, S. Huang, Y. Zhang, and X. Rao, "Experimental investigation on bubble contact diameter and bubble departure diameter in horizontal subcooled flow boiling," *International Journal of Heat and Mass Transfer*, **149**, pp. 119105 (2020).